RESILIENT INFRASTRUCTURE
June 1–4, 2016
RESILIENT INFRASTRUCTURE LONDON 2016

# IMPROVING THE EFFICIENCY OF ZINC SACRIFICIAL ANODES IN REPAIRED CONCRETE

Ahmed G. Bediwy
MSc. Student, University of Manitoba, Canada

Mohamed T. Bassuoni
Associate Professor, University of Manitoba, Canada

Martin Beaudette
Project/Testing Manager, Vector Corrosion Technologies Ltd., Winnipeg, Canada

## ABSTRACT

Zinc sacrificial anodes are considered an effective and economical method to prevent the electrochemical corrosion of steel bars by providing cathodic current to bars, which can provide corrosion protection at low galvanic current densities in the range of 0.2 to 2 mA/m$^2$. Sacrificial anodes are commonly used in RC structures particularly in bridge decks to mitigate a critical phenomenon that occurs in the original concrete beside the repaired patches, which is known as the 'halo effect'. One of the key factors affecting the efficacy of zinc anodes is the resistivity of concrete or cementitious repair material in which these anodes are embedded. There is a general notion that the higher the electrical resistivity of concrete or repair material, the less likely that zinc anodes produce the target galvanic current for optimum protection of steel bars. However, no systematic data are available on the maximum allowable electrical resistivity of repair materials/concretes beyond which zinc anodes cannot properly function to prevent corrosion. The specific objective of this study is to explore the effect of concrete resistivity on the efficiency of zinc anodes at mitigating patch accelerated corrosion (halo effect). Concrete slabs were cast to simulate the patch repair technique in the field, and the main parameter in this research was changing the resistivity of the repair section in the slabs (5,000, 15,000, and 25,000 Ω-cm). Analysis of results shows a high level of effectiveness of the anode to prevent corrosion up to 20 weeks under a wetting-drying exposure.

Keywords: Concrete; Sacrificial Anodes; Halo Effect; Resistivity.

## 1. INTRODUCTION

Corrosion of steel reinforcement embedded in concrete structures is considered as 'bottle-neck' which limits the durability and performance of reinforced concrete structures in harsh environments, and leads to significant economic and service life losses (Bentur et al. 1997). For example, some estimates state that it would cost $78 billion to restore all structurally deficient bridges in the U.S. (Whitmore and Abbott 2003). There are various techniques which have been developed to mitigate/control the damaging effect of the corrosion of steel bars in concrete such as impressed current cathodic protection (ICCP), electrochemical realkalization, and chloride extraction. Sacrificial anodes are another effective and economical method to mitigate the deleterious effects of electrochemical corrosion of steel bars, with zinc anodes being the most common type of anode used in RC structures. Sacrificial anodes are manufactured from a metal (e.g. zinc) which has a more negative electrochemical potential than that of the steel reinforcement. Due to the difference in potential between the anode and the steel, a current will be generated and flow through the electrolyte (pore solution in the case of concrete). Consequently, the steel will become more negatively charged and behave as a cathode and the anodic metal is oxidized [loses electrons/decomposes] (Wilson et al. 2013). The typical service life of sacrificial anodes is 10 to 30 years, depending on the severity of the service conditions (chloride ions loading, environmental conditions, saturation level, etc.). Aluminum, zinc, and magnesium are the most commonly used metals as sacrificial anodes. Zinc anodes have been adopted by many transportation agencies in North America due to their high efficiency in mitigating

corrosion of steel and low rate of expansion when embedded into concrete elements. Typically, they are fabricated in three different shapes a puck, cylinder and small pellet (Whitmore and Abbott 2003). Using zinc anodes in patch repairs in a RC element prevents the onset of corrosion within a surrounding area and keeps the steel in a condition of 'imperfect passivity' by providing a cathodic current to the reinforcing steel. This can be fulfilled by low densities of galvanic current in the range of 0.2 to 2 $mA/m^2$ (Pedeferri 1996). However, in many field cases, deterioration induced by reinforcement corrosion has been found in the original/parent concrete in the vicinity of repaired patches sometimes within a few months of repair operations; this critical phenomenon is known as the 'incipient anode' or 'halo effect' (Page and Sergi 2000, Christodoulou et al. 2013).

One of the key factors affecting the efficacy of zinc anodes is the resistivity of concrete or cementitious repair material in which these anodes are embedded. There is a general notion that the higher the electrical resistivity of concrete or repair material, the less likely that zinc anodes produce the target galvanic current for optimum protection of steel bars. As a result, low to moderate resistivity repair materials/concretes have been specified with zinc anodes. In North America, a resistivity value of less than 15,000 ohm-cm has been arbitrarily specified for repair patches of RC structures comprising zinc anodes (ACI RAP-8, 2010). However, no systematic data are available on the maximum allowable electrical resistivity of repair materials/concretes beyond which zinc anodes cannot produce the target galvanic current to prevent corrosion (Andrade and Alonso 1996, Otieno et al. 2010, Hornbostel et al 2013, Ahmed 2014). On the other hand, low resistivity repair materials/concretes generally have higher penetrability, which may facilitate chloride ions ingress in repaired patches and consequently aggravate the process of corrosion. Therefore, the objective of this study is to explore the effect of concrete resistivity on the efficiency of zinc anodes at mitigating patch accelerated corrosion (halo effect). This might help identifying the range of resistivity of repair materials/concrete within which zinc anodes retain their functionality.

## 2. EXPERIMENTAL PROGRAM

### 2.1 Materials

General use (GU) portland cement and silica fume (SF), which meet the requirements of CAN/CSA- A3001 (2013) were used in this study. Their chemical and physical properties are shown in Table 1. Locally available coarse aggregate (natural gravel with max. size of 9.5 mm) and fine aggregate (well graded river sand with fineness modulus of 2.9) were used. The specific gravity and absorption were 2.65 and 2%, respectively for gravel and 2.53 and 1.5%, respectively for sand. A high-range water reducing admixture (HRWRA) based on polycarboxylic acid and complying with Type F as described in ASTM C494/C494M [Standard Specification for Chemical Admixtures for Concrete] (2013) was added to all mixtures to maintain a slump range between 50 and 100 mm. In addition, an air-entraining admixture according to ASTM C233/C233M [Standard Test Method for Air-Entraining Admixtures for Concrete] (2014) was used to achieve an entrained air content of about 5-6%. Conforming to ASTM C309 (2012), a membrane curing compound was applied to prevent the loss of water from the surface of concrete at early-age and to simulate curing in the field.

Table 1: Chemical and physical properties of the cement and silica fume

| | Chemical composition (%) | | | | | | | Physical properties | |
|---|---|---|---|---|---|---|---|---|---|
| | $SiO_2$ | $Al_2O_3$ | $Fe_2O_3$ | CaO | MgO | $SO_3$ | $Na_2O$ | Fineness ($m^2/kg$) | Specific Gravity |
| GU Cement | 19.8 | 5.0 | 2.4 | 63.2 | 3.3 | 3.0 | 0.1 | 410 | 3.17 |
| Silica Fume | 92.0 | 1.0 | 1.0 | 0.3 | 0.6 | 0.2 | 0.3 | 20,000 | 2.22 |

### 2.2 Experimental Set-up

The laboratory study has been conducted on duplicate mini-scale slabs (205 mm wide × 610 mm long × 120 mm thick) poured in three sections as shown in Figure 1. The bottom half (chloride free concrete) were prepared from

normal concrete with a 28-day resistivity of approximately 5,000 ohm-cm (cement content and w/c of 300 kg/m$^3$ and 0.50, respectively), and it was reinforced with two longitudinal 750 mm #10 bars. This (parent/old) concrete mixture design is within the typical range of concrete bridge deck slabs built more than 25-35 years ago or so (Ramey et al. 1997, Feldman and Bartlett 2007). The top half was split into two equal sections: one section (old concrete: contaminated with 3% calcium chloride by mass of cement) with a resistivity of 5,000 ohm-cm, and it was reinforced with two #10 bars with 375 mm length, while the other section (repair patch-chloride free) had a varied resistivity. The reinforcement in the patched part was two #10 bars with 365 mm length, positioned to leave 10 mm gap from the bar in the adjacent chloride contaminated concrete to ease monitoring the current generated (output) from the anode to each rebar in the assembly through external wiring. All bars protruded outside the formwork by 70 mm (Figure 1).

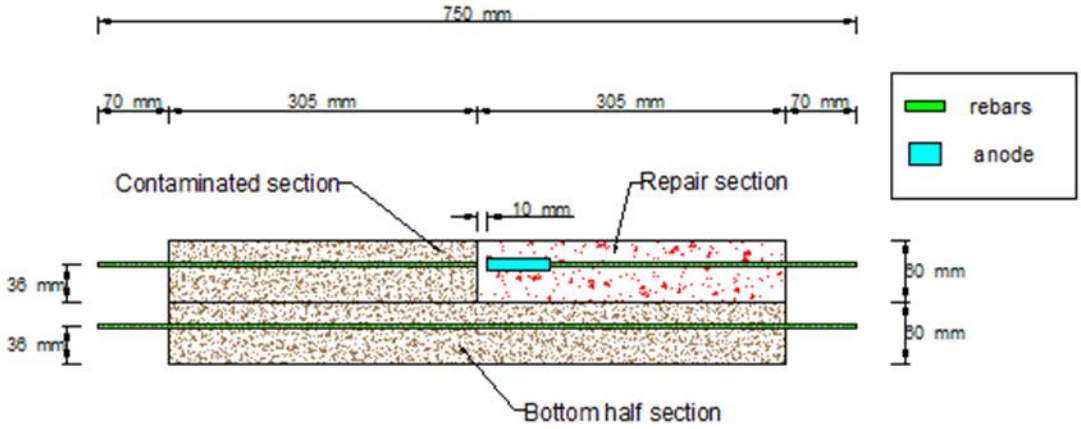


Figure 1: A schematic diagram of a cross-section from a slab specimen with the reinforcement and anode assembly.

The simulated repair sections in the slabs were prepared with three different concrete mixtures ($R_5$, $R_{15}$ and $R_{25}$) as shown in Table 2 to produce bulk electrical resistivity of 5,000, 15,000, and 25,000 ohm-cm. These mixtures were extracted from a previous study by the authors on the resistivity and penetrability of various concrete mixtures (Bedwiy and Bassuoni 2015). The zinc anodes (puck shape, Figure 2) were mounted in the repair sections at spacing of 25 mm from the bond line with the adjacent concrete. The current in the three sections has been monitored by external wire connections and electrical switches (Figure 3) to determine the current in each bar individually. To accelerate the onset of corrosion, the slabs have been exposed to continuous wetting-drying cycles. Each cycle consisted of ponding (5 to 15 mm) the surface of specimens with fresh water for two weeks at a temperature of 22±2˚C, followed by drying at 22±2˚C and 35±5% RH for two weeks. The specimens have been put in a controlled lab temperature, and a dehumidifier has been used in the drying cycles to obtain the target humidity level. Additional six slabs were cast in this study, but without zinc anodes (control slabs), to assess the functionality of zinc anodes to control electrochemical corrosion of bars.

Figure 2: Zinc sacrificial anode used in this study.

Table 2: Proportions of repair mixtures per cubic meter of concrete

| Mixture ID. | Cement (kg) | Silica Fume (kg) | Water (kg) | w/b | Coarse Agg. (kg) | Fine Agg. (kg) | HRWRA (ml/100 kg of binder) | Air-Entrainer (ml/100 kg of binder) |
|---|---|---|---|---|---|---|---|---|
| $R_5$ | 300 | - | 150 | 0.5 | 962 | 962 | 300 | 15 |
| $R_{15}$ | 400 | - | 120 | 0.3 | 986 | 986 | 937 | 20 |
| $R_{25}$ | 368 | 32 | 120 | 0.3 | 1182 | 788 | 905 | 15 |

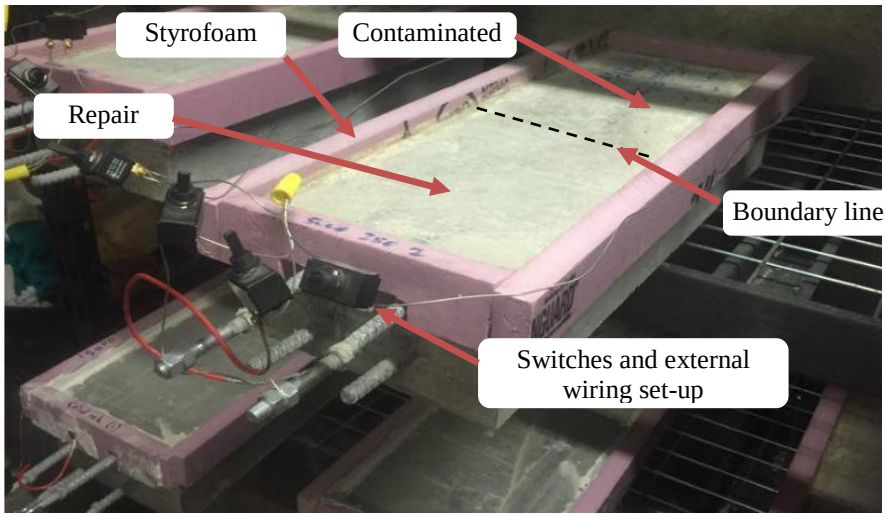


Figure 3: Full set-up of a slab specimen.

### 2.3 Tests

To verify the resistivity of the repair mixtures, quadruplicate cylindrical (100×200 mm) specimens were prepared for each mixture. The specimens were demolded after 24 h and cured in a standard curing room (maintained at a temperature of 22±2°C and relative humidity of more than 95%) until testing at 28 days. 2-pin AC resistance meter was used to determine the bulk resistivity (BR) of saturated surface dry concrete cylinders (Figure 4a). The apparatus consists of a control box, two titanium plate electrodes, and two conductor wires to connect the control box to the plates. The specimen was placed between the two plate electrodes, and an AC current (97 Hz) was applied through the specimen by the control box. To ensure appropriate electrical connection between the specimen and the plate electrodes, sponges saturated with sodium sulfate solution were inserted between the specimen and electrode plates at the top and bottom ends of the specimen. The device measured the electrical resistance by adjusting the resistance dial, located on the control box, until the null indicator is balanced in the middle. The resistance, which is measured in ohms, is the raw output from the apparatus. To calculate the electrical resistivity in ohm-cm, Eq. 1 was applied, where L is the specimen's length (cm), and A is the specimen's cross-sectional area ($cm^2$).

[1] $$\text{BulkResistivity} = \text{BulkResistance} \times \frac{A}{L}$$

The resistivity of slabs was monitored with the time of exposure (after the wetting cycles) by measuring the surface resistivity (SR) rather than the bulk resistivity because of the difficulty in positioning the bulk resistivity set-up on a flat system (such as slabs). This is the reason for commonly using SR set-ups in field applications. The SR was determined by the Wenner four-electrode method, where the four electrodes are equally spaced (38 mm) and located in a straight line. By placing the four electrodes on the surface of the concrete, the two exterior electrodes apply an AC current, while the two inner electrodes measure the electrical potential created. Subsequently, the value of SR is obtained (in ohm-cm) automatically from the control box which is connected to the four probes by a conductor wire as shown in Figure 4b. The current was measured using a precision digital multimeter (Model MAS830B, maximum capacity of 10A) every two weeks (at the end of each exposure cycle). To calculate the current density in $mA/m^2$, the reading of the current obtained from the multimeter is normalized by the outer surface area of the bars being measured, neglecting the protruded portions that were coated by epoxy. In addition, the potential of steel bars has been evaluated against portable copper-copper sulfate reference electrode (CSE) in accordance with the technique described in ASTM C876 (2009).

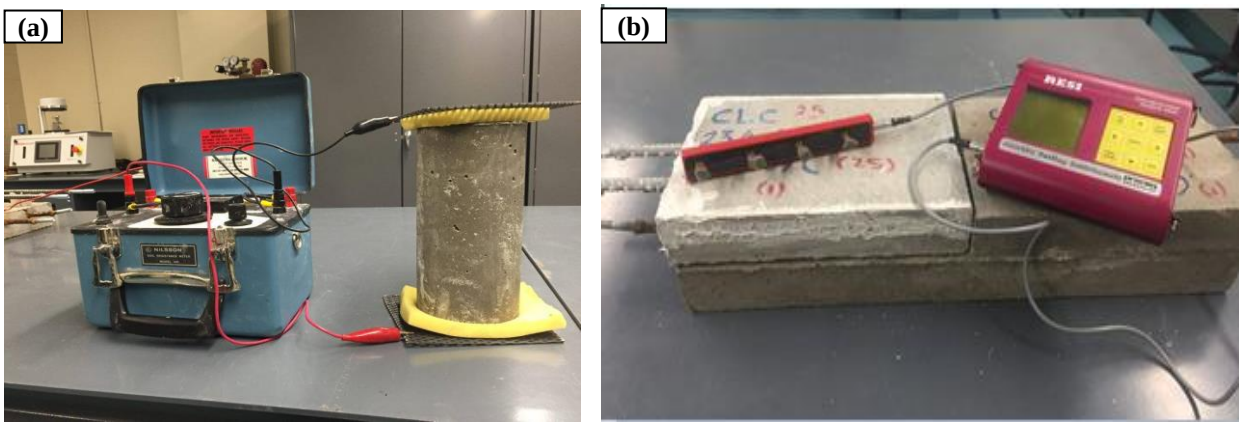


Figure 4: (a) 2-pin AC resistance test set-up, and (b) Wenner probe array test set-up.

## 3. RESULTS AND DISCUSSION

### 3.1 Resistivity

The average surface resistivity (SR) of duplicate slabs for the repair patch measured at the end of each wetting cycle is depicted in Figure 5a. However, the SR measurements tend to be 1.8 to 3.4 higher than that of the bulk resistivity (BR) of the same concrete due to electrode polarization, configuration of test-setup and contact resistance between the electrodes and the concrete (Morris et al. 1996, Polder 2001, Spragg et al. 2011, Ghosh and Quang 2014, Ghosh and Quang 2015). Consequently, a conversion factor with an average value of 2.6 has been applied in this study to obtain the BR from the SR measurements to monitor the change of resistivity with time for the repair sections containing the anodes as shown in Figure 5b. The results conform to the well-documented trend of the effect of the w/b and SCMs on the physical characteristics of the pore structure of concrete, and in turn its electrical resistivity. For example, increasing the w/b from 0.3 to 0.5 led to a marked decrease (46%) in the surface resistivity, due to the higher porosity and enhanced pore continuity of the cementitious matrix (Bassuoni and Rahman 2016). Compared to the single binder mixture ($R_{15}$; w/b = 0.3), the addition of 8% silica fume in mixture $R_{25}$ led to a significant increase in the surface resistivity of about 122 %, because of further densifying the pore structure via the pozolanic reactivity which blocks the channels for ions to go through, in addition to binding ionic species in the cementitious matrix (Lataste 2010). The slightly increasing trends of resistivity with time (Figure 5a-b) for all the mixtures are attributed to the progression of the hydration process in the repair sections, especially with the exposure regime adopted in this study, which has wetting cycles with pure water stimulating renewed curing of concrete (in addition to aggravating the corrosion of bars).

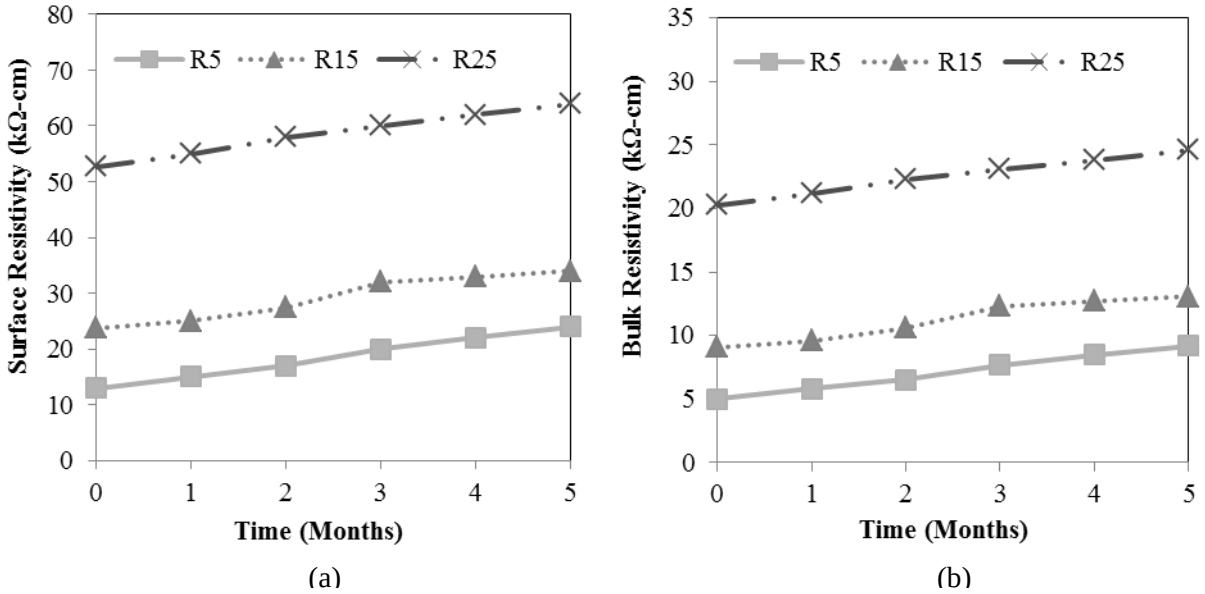


Figure 5: Resistivity of the repair sections after the wetting cycles: (a) surface resistivity (SR), and (b) bulk resistivity (BR).

### 3.2 Current Measurements

The total current from the anode (Figure 6a) was almost equal to the summation of the current in the individual bars embedded in all three sections, which verified that the anode's current had been well distributed to all three sections without significant losses. In addition, Figure 6b shows the current density, which reflects the change of the total current originating from the anode normalized by the surface area of the steel bars with time. The total current increased and reached its peaks when the slabs were wetted, which could be explained by the ease of mobility of ionic species through the pore structure with saturation. The trend of the current measurements (Figures 6a-b) is consistent with the resistivity of the repair sections (Figures 5a-b) in the sense that concrete with higher resistivity

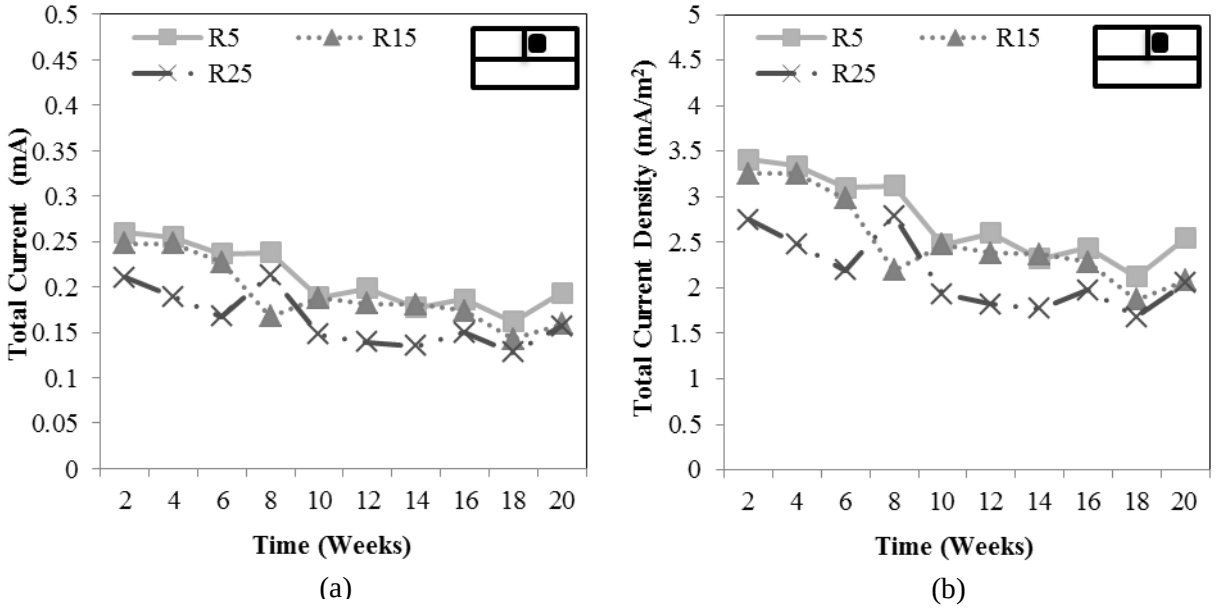


Figure 6: Change in the (a) total current, and (b) current density of the zinc anodes in the repair section.

had lower current density and vice versa. For example, increasing the resistivity of the repair sections, in which the anodes are embedded, from 5,000 to 25,000 ohm-cm led to a reduction of 29% in the total current density of the zinc anode. This can be attributed to restricted migration of the ionic current through the electrolyte in capillary pores.In the beginning of exposure, the maturity of the concrete was still low, resulting in high current densities (2.75 to 3.5 $mA/m^2$) for all resistivity values; however, all these values decreased with time due to the development of microstructure (i.e. higher maturity). Because of the ascending trend of the resistivity with time (Figures 5a-b), the current densities exhibited a slight and continuous reduction relative to their initial values. Nevertheless, the current from the zinc anodes has remained above the level believed to be adequate for cathodic prevention, which alludes to the functionality of zinc anodes so far in high resistivity concrete (up to 25,000 ohm-cm) within the exposure period of 20 weeks.

### 3.3 Half-cell potential

The change in potentials for the bars in the repair and chloride contaminated sections of the control (without anodes) $R_5$, $R_{15}$, and $R_{25}$ slabs with time are shown Figures 7a-b. The bars in the repair sections showed potential readings ranging between -100 to -300, -175 to -250, and -160 to -230 mV vs CSE for the $R_5$, $R_{15}$, and $R_{25}$ slabs, respectively within the exposure period of 20 weeks. As expected, the average of these ranges is almost higher (more positive) than -200 mV vs CSE, which indicates that the likelihood of corrosion activity of steel bars in the repair sections is less than 10%, according to the potential thresholds stipulated in the ASTM C876 (2009). With the increase of resistivity, the variability between the peaks of the potential measurements associated with wetting-drying cycles was reduced (Figure 7a). This may be ascribed to the densification of the pore structure ($R_{15}$ and $R_{25}$ slabs) associated with the reduction of w/b and/or incorporation of silica fume as explained in Section 3.1. Moisture transport in such matrices occurs at slower diffusion rates (Mehta and Monteiro 2014), which may not allow significant evaporation of water during the drying cycles, and thus the moisture states in the wetting-drying cycles were comparable which reduced the variability in the potential readings for these slabs. In contrast, the slab with low resistivity ($R_5$), which had an open pore structure allowed for easier moisture transport; thus, considerable evaporation during the drying cycles led to reduction of corrosion activity, as indicated by the significant shift of the potentials upwards (towards the less negative values).

On the other hand, the bars in the chloride contaminated sections (Figure 7b) yielded more negative values than that of the corresponding ones in the repair sections (Figure 7a). It should be emphasized that the contaminated sections in all slabs were prepared from normal concrete with a 28-day resistivity of approximately 5,000 ohm-cm, and it seems that changing the resistivity of the repair sections did not significantly affect the corrosion activity in the contaminated sections as the trends were comparable in Figure 7b. On average, the potential measurements in the contaminated sections were nearly more negative than -350 mV vs CSE for all resistivity values. Thus, as expected, the likelihood of corrosion activity in this section is high (more than 90% according to ASTM C876). Because of the differences in potentials between the repair and chloride contaminated sections, the boundary zone is susceptible to the incipient anode phenomenon (halo effect) as intended in the design of the test set-up. The potentials for all three resistivity values showed a progressive trend with time towards the range where the corrosion activity is uncertain (between -200 and -350 mV vs CSE according to ASTM C876) which can be ascribed to the continual hydration of concrete as reflected by the increase in resistivity with time (Figures 5a-b). Unlike the potential measurements for the bars in the repair section of R5, the variability between the peaks of the potential measurements (associated with wetting-drying cycles) in the corresponding contaminated section was reduced. This might be due to the increased moisture level in the contaminated section (i.e. inadequate evaporation during the drying cycles) due to the availability of a salt solution in the matrix (admixed calcium chloride dissolved in water) rather than fresh water (the case for the repair section). Figure 8 shows the average potential for the whole slabs without and with anodes. The in-progress results indicate that the slabs with anodes yielded more negative values so far in comparison to the counterpart slabs without anodes, which were -259, -248, and -261 mV vs CSE for the $R_5$, $R_{15}$, and $R_{25}$ slabs, respectively. This is resulting from the current flowing to the steel from the anode, polarising the steel, which links to the trends in Figures 6a-b.

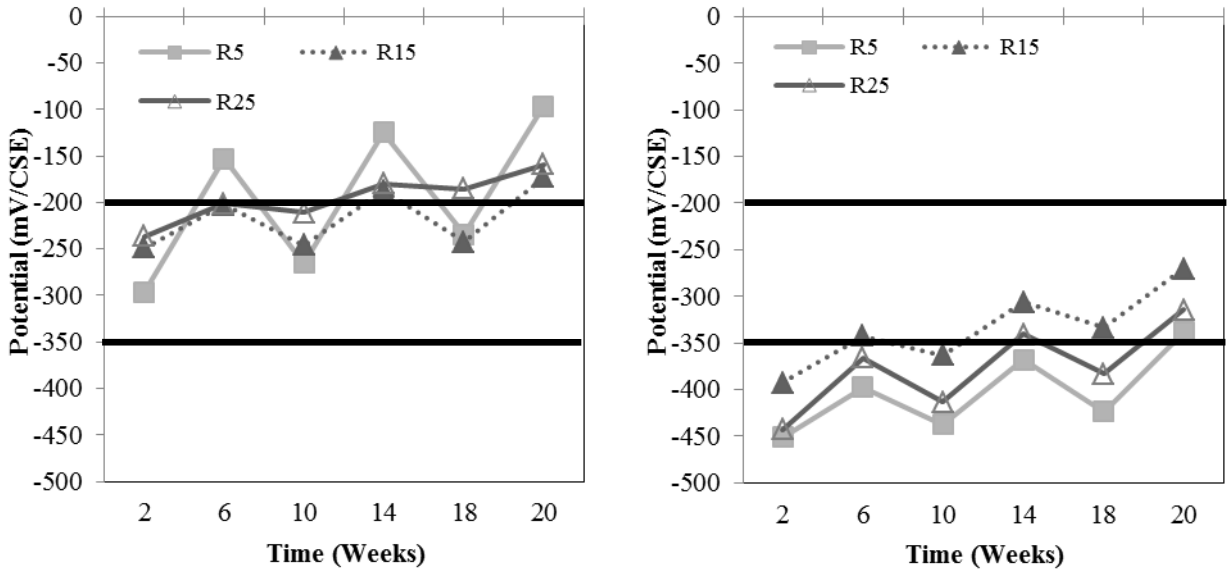


Figure 7: Potential of steel bars in slabs without anodes: (a) repair sections, and (b) chloride contaminated sections.

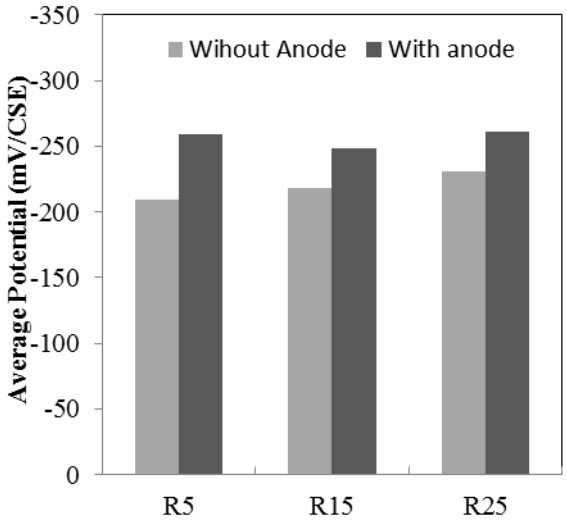


Figure 8: Average potentials of slabs without and with zinc anodes.

## 4. CONCLUSIONS

Considering the test-setup, resistivity of the repair sections, testing methods, and exposure period implemented in the current study, the following conclusions can be drawn:

- The results of resistivity of concrete conformed to the well-documented trends of the effects of w/b and SCMs. In addition to the effect of continual hydration with time, reduction of w/b from 0.5 to 0.3 and incorporation of 8% silica fume led to increasing the resistivity of the repair sections from 5,000 to 25,000 ohm-cm due to densification of the pore structure, in addition to binding ionic species into the cementitious matrix in the case of silica fume.

- The slab configuration designed in the current study was capable of stimulating the incipient anode phenomenon (halo effect) as reflected by the differences in potentials between the repair and chloride contaminated sections, irrespective of the resistivity value of the repair section.
- In-progress results showed that the total current density originating from the anode has been distributed over the bars in all sections and remained above the acceptable level (0.2 to 2 $mA/m^2$) to prevent corrosion even with the high resistivity concrete (25,000 ohm-cm).
- In-progress results indicate that the slabs with anodes yielded more negative potential measurements in comparison to the corresponding slabs without anodes, as a result of the current flowing to the steel from the anodes.
- At this preliminary stage, the overall results allude to the functionality of the zinc anodes up to 20 weeks of exposure involving repetitive wetting-drying cycles; however, the exposure period should be extended to obtain conclusive trends, which is currently underway.

## ACKNOWLEDGEMENTS

The authors highly appreciate the financial support from Natural Sciences and Engineering Research Council of Canada and sponsorship from Vector Corrsion Technologies Ltd . The new IKO Construction Materials Testing Facility at the University of Manitoba in which these experiments were conducted has been instrumental to this research.

## REFERENCES

ACI Committee E706, ACI RAP Bulletin-8 2010. Installation of Embedded Galvanic Anodes. *American Concrete Institute*, Farmington Hills, MI, 7 p.

Ahmad, S. 2014. An Experimental Study on Correlation between Concrete Resistivity and Reinforcement Corrosion Rate. *Anti-Corrosion Methods and Materials*, 61(3): 158–165.

Andrade, C. and Alonso, C. 1996. Corrosion Rate Monitoring in the Laboratory and on-Site. *Construction and Building Materials*, 10(5): 315–28.

ASTM C233. 2014. Standard Test Method for Air-Entraining Admixtures for Concrete. *Annual Book of American Society for Testing Materials*, Philadelphia, Sec. 4, 4.02.

ASTM C309. 2012. Standard Specification for Liquid Membrane-Forming Compounds for Curing Concrete. *Annual Book of American Society for Testing Materials*, Philadelphia, Sec. 4, 4.02

ASTM C494. 2012. Standard Specification for Chemical Admixtures for Concrete. *Annual Book of American Society for Testing Materials*, Philadelphia, Sec. 4, 4.02.

ASTM C876. 2009 .Standard Test Method for Corrosion Potentials of Uncoated Reinforcing Steel in Concrete. *Annual Book of American Society for Testing Materials*, Philadelphia, Sec. 4, 4.02

Bassuoni, M. T. and Rahman, M. M. 2016. Response of Concrete to Accelerated Physical Salt Attack Exposure. *Cement and Concrete Research*, 79: 395-408.

Bediwy, A. G. and Bessuoni, M. T. 2015. A Comparative Study on Resistivity and Penetrability of Concrete. *14th international Conference on Structural and Geotechnical Engineering*, Ain Shams University, Cairo, Egypt, 10 p.

Bentur, A. Diamond, S. and Berke, N. S. 1997. *Steel Corrosion in Concrete: Fundamentals and Civil Engineering Practice*, E and FN Spon, London, UK.

CAN/CSA-A3001 2013. Cementitious Materials for Use in Concrete. *Canadian Standards Association*, CSA, Mississauga, Ontario, Canada.

Christodoulou, C. C. Goodier, S. Austin, J. and Glass, G. K. 2013. Diagnosing the Cause of Incipient Anodes in Repaired Reinforced Concrete Structures. *Corrosion Science*, 69: 123–129.

Feldman, L. R. and Bartlett, F. M. 2007. Bond Stresses along Plain Steel Reinforcing Bars in Pullout Specimens. *ACI Structural Journal*, 104(6): 685–692.

Ghosh, P. and Tran, Q. 2014. Correlation between Bulk and Surface Resistivity of Concrete. *International Journal of Concrete Structures and Materials*, 9(1): 119–132.

Ghosh, P. and Tran, Q. 2015. Influence of Parameters on Surface Resistivity of Concrete. *Cement and Concrete Composites*, 62: 134–145.

Hornbostel, K. Claus, K. L. and Mette, R. G. 2013. Relationship between Concrete Resistivity and Corrosion Rate - A Literature Review. *Cement and Concrete Composites*, 39: 60–72.

Lataste, J. F. Sirieix, D. B. and Frappa. 2003. Electrical Resistivity Measurement Applied to Cracking Assessment on Reinforced Concrete Structures in Civil Engineering. *NDT and E International*, 36: 383–394.

Lataste, J. 2010. Electrical resistivity for the Evaluation of Reinforced Concrete Structures, In: Maierhofer C, Reinhardt H-W and Dobmann G, editors, Non-Destructive Evaluation of Reinforced Concrete Structures, Woodhead Publishing Series in Civil and Structural Engineering, 2: 243–275.

Mehta, P.K. and Monteiro, P.J.M. 2014. *Concrete*, McGraw Hill Education, USA.

Morris, W. Moreno, E. I. and. Sagüés, A. A. 1996. Practical Evaluation of Resistivity of Concrete in Test Cylinders Using a Wenner Array Probe. *Cement and Concrete Research*, 26(12): 1779–87.

Page, C. L. and Sergi, G. 2000. Development in Cathodic Protection Applied to Reinforced Concrete. *Journal of Materials in Civil Engineering*, 12 (1): 8–15.

Otieno, M. B., Alexander, M. G. and Beushausen, H. D. 2010. Suitability of Various Measurement Techniques for Assessing Corrosion in Cracked Concrete. *ACI Materials Journal*, 107(5): 481–489.

Pedeferri, P. 1996. Cathodic Protection and Cathodic Prevention. *Construction and Building Materials*, 10(5): 391–402.

Polder, R. B. 2001. Test Methods for on Site Measurement of Resistivity of Concrete - a RILEM TC-154 Technical Recommendation. *Construction and Building Materials*, 15(3): 125–131.

Ramey, G. Pittman, D. W. Greg, W. and Carden, A. 1997. Use of Shrinkage Compensating Cement in Bridge Decks. Final Report on Highway Research Center Research Project, Department of Civil Engineering, Auburn University.

Spragg, R., Castro, J., Nantung, T., Parades, M., and Weiss, W. J. 2011. Variability Analysis of the Bulk Resistivity Measured Using Concrete Cylinders. JTRP Rep. SPR-3509, FHWA/IN/JTRP-2011/21, Joint Transportation Research Program, Indiana Dept. of Transportation and Purdue Univ., West Lafayette, IN.

Whitmore, D., and Abbott, S. 2003. Embedded Galvanic Anodes Increase Sustainability of Reinforced Concrete Structures. *Annual Conference of the Transportation Association of Canada*, St. John's, Newfoundland and Labrador, 10 p.

Wilson, K. Jawed, M. and Ngala, V. 2013. The Selection and Use of Cathodic Protection Systems for the Repair of Reinforced Concrete Structures. *Construction and Building Materials*, 39: 19–25.